Q. J. R. Meteorol. Soc. (2003), **1**, pp. 1–23

Simultaneous radar and aircraft observations of mixed-phase cloud at the 100-m-scale

By P. R. Field[1]* , R. J. Hogan[2], P.R.A Brown[1], A.J. Illingworth[2], T.W. Choularton[3], P. H. Kaye[4], E. Hirst[4] and R. Greenaway[4]

[1] *Met Office, UK;* [2] *University of Reading;* [3] *UMIST;* [4] *University of Hertfordshire.*

DRAFT V4.0 7/11/2003

Summary

Three UK C-130 aircraft flights performed in conjunction with the Chilbolton Advanced Meteorological Radar were carried out in mixed-phase clouds. The aircraft instrumentation included the Small Ice Detector (SID) and Nevzorov probe that are both capable of discriminating between liquid and ice phase. It was found that particle sphericity measured by SID could be successfully used as a proxy for particle phase. Using a combination of SID and other probes it is possible to determine whether a 100m cloud segment is ice, liquid or mixed-phase. Regions as short as 100 m exhibited mixed-phase characteristics. There was generally good agreement between water phase indicated by the SID and Nevzorov probes with any differences arising from the fact that the SID provides a number weighted estimate of dominant phase, while the Nevzorov probe provides a mass weighted estimate. The radar and aircraft observations show that when high values of differential reflectivity are observed the nearby presence of liquid water is indicated. When large ice crystals are present in deeper cloud they can supress the differential reflectivity signal. Therefore the absence of a high differential reflectivity signal does not necessarily mean that liquid water is absent.

Keywords: mixed-phase radar aircraft

1. Introduction

Observations of mixed-phase cloud have been hampered by the lack of instrumentation capable of determining the phase of particles and have relied upon manual or automatic techniques of identifying optical array probe 2D images, which is only feasible for particles larger than 125 μm, or manual analysis of impactor data. Recently, analysis of mixed-phase clouds has been carried out utilising the Nevzorov hotwire probe, the Rosemount Icing Detector (Cober et al., 2001; Korolev et al., 2003) and an airborne nephelometer (Jourden et al. 2003). Korolev et al. (2003) showed that ratio of ice water content to total condensed water content was usually either greater than 0.9 or less than 0.1 for ~100m horizontal regions with a minimum for intermediate values of this ratio. They observed concentrations (1 Hz) of ice particles for temperatures colder than -10C in the range 2–5 cm^{-3} using two FSSPs. In clouds defined as containing only liquid droplets, the concentrations (1 Hz) were found to decrease from ~200 cm^{-3} at -10C to ~30 cm^{-3} at -35C. Cober et al. (2001) found that FSSP median volume diameters were always greater than 30μm when ice was present. Jourden et al. (2003) present results from a polar nephelometer where prinicple component analysis of 28 scattering angles between 4 and 170 deg were used to determine whether a 100m interval was liquid, ice or mixed-phase. They went on to invert the measured scattering function to retrieve liquid

* Corresponding author: Met Office, Building Y46, Cody Technology Park,Ively Road, Farnborough, Hampshire, GU14 0LX, UK. e-mail: paul.field@metoffice.com

and ice size distributions given a priori scattering functions for liquid and ice.

This paper presents observations from three flights carried out in mixed-phase cloud in concert with ground based radar observations from the Chilbolton 3-GHz radar in the UK. Understanding the disposition of ice and liquid in mixed-phase cloud is important for predicting the radiative impact of mixed-phase clouds, the evolution of precipitation systems, the sub-grid numerical weather model representation of mixed-phase conditions and has implications for predicting the occurrence and severity of aircraft icing.

The Chilbolton radar has the capability of detecting polarised reflectivity signals. This ability has been used in previous radar-aircraft studies to show that the differential reflectivity, Z_{DR}, (the ratio of the horizontally and vertically polarised Reflectivity signals) can exhibit high values in the vicinity of supercooled liquid water (Hogan et al. 2002, 2003). The conditions of high supersaturation with respect to ice lead to the rapid growth of pristine ice crystals. Large ZDR values can arise if these crystals have large axial ratios and are horizontally aligned as they fall. Thus the ZDR signal can act as a 'tell-tale' for the presence of supercooled liquid water if pristine crystals that develop large axial ratios dominate the radar signal, although as shown by Hogan et al. (2002), the finite fall speed of the ice means that the high ZDR and supercooled water regions may not be precisely colocated.

The purpose of this paper is firstly to examine the response of SID to enable rigorous definitions of ice, liquid and mixed-phase cloud to be obtained. These definitions will then be used to examine 100-m scale observations from a variety of cases. These observations will be compared with those from radar. It is the intention of this paper to convey the complexity of mixed-phase clouds, so we will describe the high resolution (100-m scale) structure of mixed-phase regions by comparing the radar and aircraft data. The complexity is derived from the observations provided by varied probes we have made use of and we must describe and intercompare their responses to place the observations in the proper context. Therefore, we will also attempt to assess the phase discriminating abilities of the Small Ice Detector and Nevzorov probes. Further interpretation of the microphysical and dynamical processes that produce the observed structures will be provided in a companion paper that utilises a Cloud Resolving Model.

In the next section the instrumentation is briefly described. The methods used to determine phase are outlined in section 3. Section 4 contain sketches of the meteorological situations encountered. Section 5 describes the responses of various aircraft instrumentation to mixed-phase conditions and compares different ways of assessing phase. Section 6 combines the radar and aircraft observations and section 7 discusses the observations from the three flights. A summary and conclusion is provided in section 8.

2. Instrumentation

The ground based radar is the 3-GHz Chilbolton Advanced Meteorological Radar. It has a large 25 m antenna that provides both high sensitivity and narrow beam width (0.28deg 1-way full width half maximum). The radar gate length is 300m and at 60 km the beam width is also ~300 m. The integration time is 0.25s. It is also capable of transmitting and receiving polarised signals enabling differential reflectivity to be studied. Hogan et al. (2002) describe the analysis of this type of data in a previous mixed-phase study carried out in tandem with the C-130. A complete description of the capabilities

of the radar is given by Goddard et al.(1994).

The Met Office C-130 instrumented aircraft was used for in situ characterisation of the microphysics. Large hydrometeors were detected with the Particle Measuring Systems 2D-C (25-800μm) and 2D-P (200-6400μm) optical array probes (Knollenberg, 1970). The processing of the 2D imagery follows that described by Moss and Johnson (1994). Small particle concentrations were estimated with a fast FSSP (Dye and Baumgardner 1984) and a Small Ice Detector (SID, Hirst et al., 2001). The observations obtained from the FSSP and SID have to be considered with care in these mixed-phase flights. In regions where large ice crystals are present the FSSP detects a bimodal distribution of interarrival times which may be caused by particle breakup on the inlet tubes of the instruments (see Field et al. 2003). However while artificial breakup may enhance the numbers of ice crystals detected by these two probes, this should not affect the detection and counting of liquid droplets. A Nevzorov probe was used to detect total condensed water and liquid water content (Korolev et al., 1998). A Lyman-α evaporative probe (Nichols et al. 1990) was used to measure total water content (Q_t, vapour+condensed water) and provide an independent estimate of ice water content (later denoted as IWC_{Q_t}). The absolute accuracy of Q_t is of the order of 5% (Wood and Field 2000). The SID probe was also used to determine the dominant phase of the particles in the sub $\sim$50μm size range. All measured values reported in this paper are 1-s averages ($\sim$100 m horizontal distance) unless otherwise stated.

3. Phase determination

The hypothesis that liquid droplets are spherical and ice crystals are not spherical is the basis of the phase determination method used by the SID probe. SID is a laser scattering device that can count and size spherical particles between 1 and 35 μm (diameter) and count non-spherical particles. The probe uses six detectors arranged azimuthally at a forward scattering angle of 30°, with a seventh detector mounted at the forward scattering angle. One of the six 30° detectors has an iris fitted to allow it to define a 400x800μm ellipse on the scattering laser. When light was detected by this detector and one other detector, a particle was known to be in the sample volume and the detector responses were recorded. By comparing the responses of the azimuthally arranged detectors an 'asphericity factor' (Af) could be obtained for each particle measured that ranges from 0 for spherical particles to 100 for very non-spherical particles (see Hirst et al. 2001 for more details). The five 30° detectors that were not stopped down with the iris were used to compute Af using:

$$Af = k\frac{\sqrt{\sum_{i=1}^{5}\left(< E > -E_i\right)^2}}{< E >}, \qquad (1)$$

where k is a constant (=22.361) set to place Af in the range 0-100, E_i are the detector values and $< E >$ is the mean of E_i. In practice, noise and differences between the detectors mean that the spherical droplets that should give $Af = 0$ will in general produce non-zero values. Single particles must therefore be differentiated from ice by using a threshold value for the asphericity.

We have used reference sets of data from warm stratocumulus (T>0C, 3.6x10^6 particles) and cold cirrus (T<-40C, 10^5 particles) to assess the range of Af values encountered in pure liquid and pure ice cases. It is seen that in practice there is a small proportion

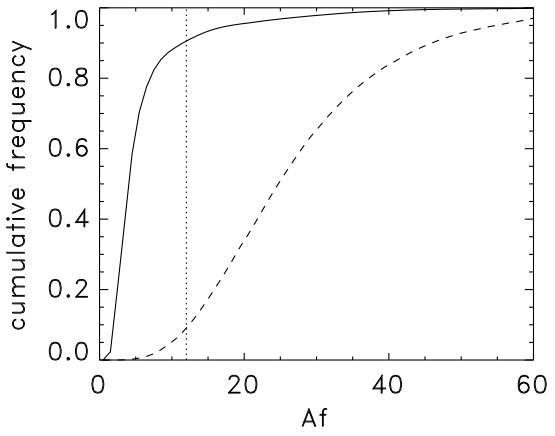

Figure 1. Cumulative frequencies of SID asphericity (Af) values obtained on flight legs with T>0C (Solid) and T<-40C (dashed). The vertical dotted line represents a spherical/non-spherical particle threshold (Af=12). Based on these datasets, in liquid cloud conditions 90% of particles have $Af < 12$ and in glaciated cloud conditions 90% of particles have $Af > 12$).

of liquid particles that exhibit high Af values (see fig 1). We believe this is due to geometrical configuration of the detector volumes when large droplets are present. This was confirmed in the laboratory by probing the edge of the sample volume with an optical fibre. There is also a proportion of ice particles that have low Af values. Variations in the ice Af values may be related to particle habit. The wide range of Af values means that it is difficult to determine with certainty whether a single particle is liquid or ice from a measurement of Af alone. If we plot SID spherical fraction, that is the fraction of particles in 1-s with $Af < 12$, we expect to get values of $\sim$0.9 for pure liquid cases and $\sim$0.1 for pure glaciated cases. In Hirst et al. (2001) a threshold value of 7 was chosen based on laboratory work that made use of 3 μm diameter latex spheres at much lower sample speeds. The threshold value of 12 was chosen because it conveniently defines 90% of both liquid and ice particles based on the insitu aircraft sampled reference datasets used here.

The method used here to determine the dominant phase for a 1-s period uses the distribution of Af values (Af bins 1-unit wide) obtained in each 1-s period. A cumulative frequency histogram is computed (using a minimum of 5 particles : 0.2 cm^{-3}) and then compared with the two reference cumulative frequency curves for assumed ice only and liquid only conditions using a Kolmogorov-Smirnov test . The Kolmogorov-Smirnov test statistic is found by examining the difference between the reference curve and the measured curve in each Af bin. The largest difference is the test result. The reference curve that gives the lowest statistic from the Kolmogorov-Smirnov test when compared with the measured distribution is the closest match to the measured distribution. The test determines whether the observed distribution is closest to the ice or liquid reference curve and hence defines the phase for that 1-s ($\sim$100 m) period.

Using this method provides an estimate of the number weighted dominant phase in the sub $\sim$50 μm size range for every 100 m of horizontal flight. Figure 2 shows two

examples of the comparison of actual 1-s Af cumulative frequencies with the test distributions. Figure 2a shows the individual particle Af values as a function of run time. Panel b shows that the cumulative histogram obtained at time=100s is closest to the ice test distribution and so this 1-s interval is designated as being ice dominated in the SID size range. In panel c the measured cumulative distribution at time=450s is closest to the liquid test curve and so the 1-s interval is determined to be liquid dominated in the SID size range. Figure 2d shows the SID phase determination along the run in 1-s intervals. Initially the run is dominated by ice and finishes in cloud dominated by liquid in the SID size range with some small pulses of liquid observed near the middle of the run. This phase determination is only valid in the $<\sim 50\mu$m size range. Thus, if the SID determines a 1-s interval to be liquid there may also be larger ice particles present that during the same period that will mean the interval is really mixed-phase.

The Nevzorov probe is a combination of two hot wire probes: a total condensed water probe (NTW Nevzorov Total Water) and a liquid water probe (NLW Nevzorov Liquid Water). The NTW part of the probe has the hot wire wound into a conical cup that faces into the airflow and captures both ice and water. The NLW part of the probe has the hot wire wound around a pole and is similar in dimensions to the King liquid water probe. The NLW should capture only liquid with the ice particles merely bouncing off. Therefore by comparing the NLW and NTW signals from the Nevzorov probe it should be possible to determine a mass weighted phase (see Korolev et al. 1998, 2003). It is estimated that the bulk water error on a 1-s measurement is 20% (Korolev et al. 1998). We have also assumed a noise threshold of 0.01 g kg^{-1} for these probes on a 1-s measurement. Values below 0.01 g kg^{-1} have been treated as zeros. In practice there are problems such as variations in the collection efficiencies of the probes. When the bulk of the water mass is located in small droplets the NLW will exceed the NTW and vise versa when the mass is located in larger droplets (see Strapp et al. 2003). A further complication is that the NLW shows a 'residual' signal in pure ice conditions caused by small ice particles sticking to the NLW sensor windings (NLW=0.11×NTW when only ice is present, Korolev et al. 1998) The problems involved in using these probes to determine phase shall be explored in the next section.

4. General Meteorological Situations

The synoptic situation for the 20th October 2000 (A803) featured a weak low to the west of Ireland that tracked northwards throughout the day. The associated front trails along the west of the mainland UK bringing rain and strengthening winds to western and central parts of the UK. Radar network imagery showed two distinct bands of precipitation to the west of Chilbolton which were moving to the NNE, associated with a cold front. The ice feeding the precipitation extended towards Chilbolton, up to an altitude of 10 km, and through the day the ice cloud base descended until 16:30 UTC when rain was detected at the surface at Chilbolton. Aircraft sampling was carried out between 4 km (-10C) and 7.5 km (-32C)to the west of Chilbolton out to a range of $\sim$70 km.

On the 21st November 2000 (A806) a warm front was occluding as it moved into the south west of the UK bringing rain ahead of it. A broad band of precipitation swept across southern England from a south-westerly direction, and rain was first measured at Chilbolton at 13:45 UTC. Aircraft sampling was carried out between 3 km (-6C) and 5

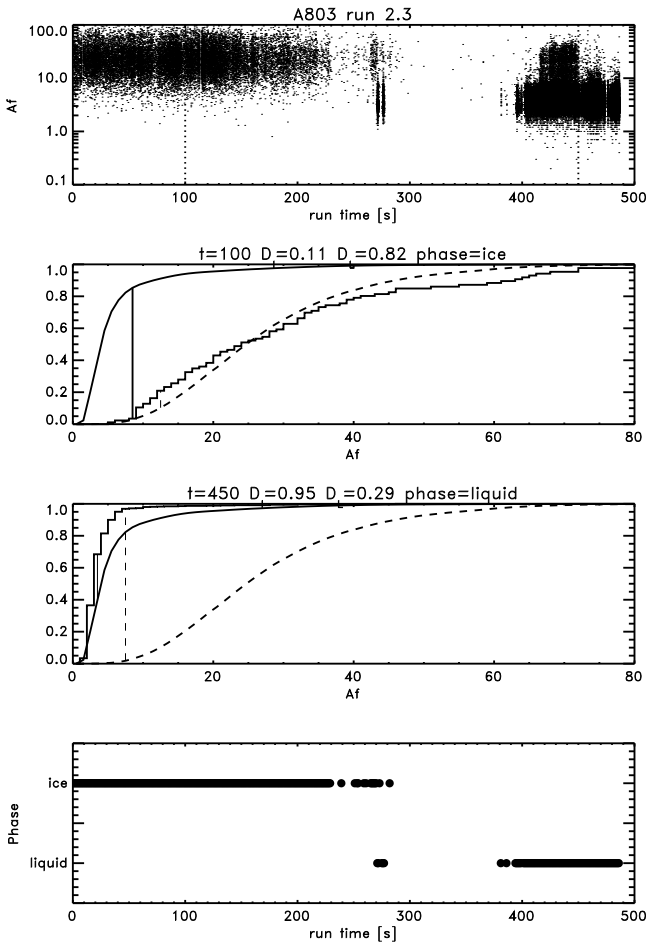

Figure 2. Example of SID phase determination. a) shows Af values as a function of run time for each particle measured. b) shows the two reference Af cumulative distributions (solid:liquid, dashed:ice) and a 1-s cumulative distribution at run time =100s (stepped line). The vertical lines between the reference distributions and the measured distribution are a graphical representation of the Kolmorogov-Smirnov statistic. They mark the largest separation between the measured and reference distributions. For this case the Kolmorogov-Smirnov test indicates that the measured distribution is closest to the ice reference distribution. c) Similar to b) but the distribution is for run time = 450s. In this case the test indicates that the measured distribution is closest to the liquid reference distribution. d) Shows the phase determination for each 1s interval for this run.

km (-15C)to the west of Chilbolton out to a range of ~90 km.

The synoptic situation for 28th February 2001 (A819) showed a low centred over northern France. An occlusion lying across Wales and central England moved slowly south eastward throughout the day and a trough affected south east England. Wintry showers affected England and Wales throughout the day. The cloud observed on this day occurred almost exclusively below 2.5 km and was associated with a well-mixed cloudy boundary layer. The temperature at the surface was around 0 degrees, and at cloud top was around -12 degrees. Later in the experiment the cloud measured by the Chilbolton radar began to break up. Aircraft sampling was carried out between 1 km (-4C) and 2 km (-10C)to the west of Chilbolton out to a range of ~90 km.

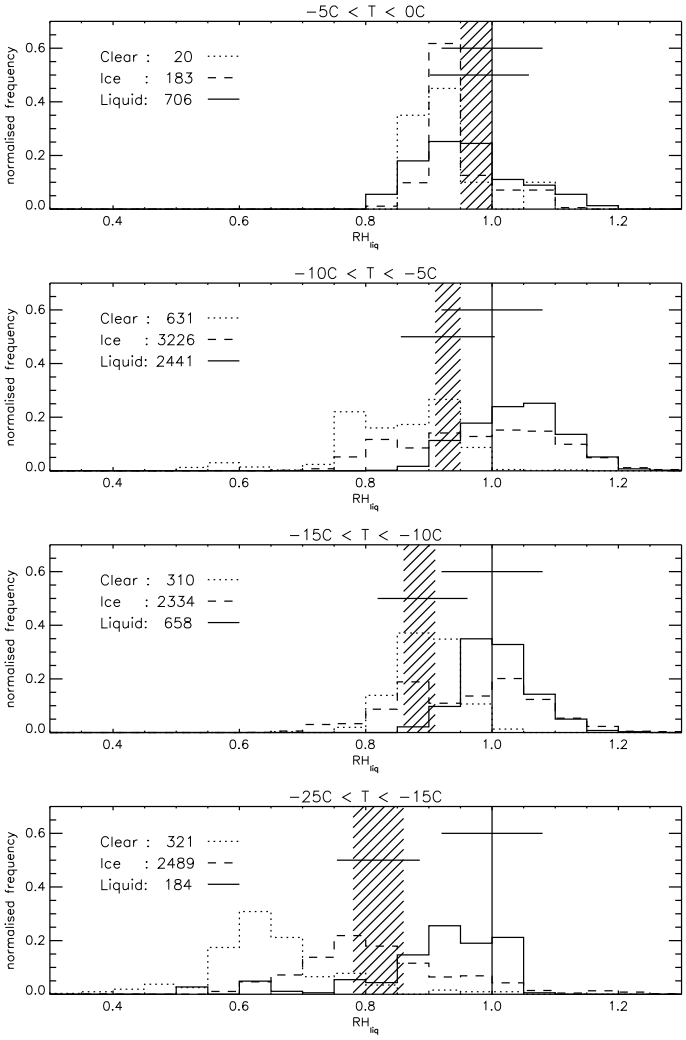

Figure 3. Plots of normalised frequency distributions of 1-s relative humidity with respect to liquid obtained from the three flights for four temperature ranges. The hatched region marks the minimum and maximum range of ice saturation for the temperature range considered. The number of points in each histogram is given in each panel. The estimated one standard deviation of the relative humidity measurements are given centred on water saturation and the middle of the ice saturation range. The solid line represents points determined to contain liquid cloud. The dashed line represents points determined to be ice cloud. The dotted line represents points in clear air (SID concentration < 0.2 cm^{-3}).

5. Probe response to mixed phase conditions

In this section we will look at the response of the aircraft probes to mixed-phase conditions in order to help interpretation of runs in the detailed comparison with the radar observations. From the three flights 25 runs were analysed totalling some 1500 km of along track distance, including ∼1200 km of 'cloudy' 100 m intervals with SID concentrations exceeding 0.2 cm^{-3}.

Before looking explicitly at the SID and Nevzorov probe data we wish to draw attention to the limitations of the relative humidity data that we will also be using in

the analysis. We have collated 1-s relative humidity information (fig 3) from the three flights to look at the distribution of relative humidity in cloudy (SID 1-s concentration ≥ 0.2 cm^{-3}) and non-cloudy conditions (SID 1-s concentration < 0.2 cm^{-3}) for four temperature ranges. The relative humidity is computed using

$$RH = \frac{Q_t - NTW}{Q_{sat}} \tag{2}$$

where Q_{sat} is the saturated specific humidity with respect to liquid and Q_t is measured directly with the Met. Research Flight Lyman-α evaporative Total Water Content probe mentioned in section 2. We can estimate the error for RH through the propagation of errors.

$$\frac{\sigma^2_{RH}}{RH^2} = \frac{\sigma^2_{Qt}}{(Qt - NTW)^2} + \frac{\sigma^2_{NTW}}{(Qt - NTW)^2} + \frac{\sigma^2_{Qsat}}{Qsat^2} \approx \frac{\sigma^2_{Qt}}{Qt^2} + \frac{\sigma^2_{NTW}}{Qt^2} + \frac{\sigma^2_{Qsat}}{Qsat^2} \tag{3}$$

Given typical errors quoted above and conditions in the troposphere for temperatures between 0C and -25C, the terms contribute respectively $(0.05)^2$, $(0.02)^2$ and for a nominal temperature error of 0.5K the last term contributes $(0.05)^2$. Therefore the predicted error is 7%

The data where liquid is present should have a relative humidity of 1. For the four temperature ranges considered, 0 to -5C, -5 to -10C, -10 to -15C, -15 to -25C, the mean and standard deviations are 0.96±0.07, 1.04±0.08, 1.00±0.06 and 0.89±0.11, respectively. For all of the liquid points taken together the mean and standard deviation are 1.01±0.09. These standard errors on 1-s relative humidity estimates in cloudy conditions derive from the combination of errors in eq. 2 and are close to the predicted value.

The top panel in fig. 3 is for the warmest temperatures (0C to -5C) where the ice saturation is close to water saturation and it is difficult to discern any significant difference between the histograms. The second panel (-5C to -10C) shows that the clear air points have humidities at and below ice saturation. The ice cloud histogram is broader than the liquid cloud histogram and extends to humidities below ice saturation. The third panel (-10C to -15C) is similar to the second panel, but clearly shows that ice cloud points have humidities ranging from ice saturation to water saturation. The last panel (-15C to -25C) shows a wide separation in the histograms with clear air points mostly subsaturated with respect to ice. Most of the ice cloud points are close to ice saturation with some at water saturation. When ice is present the relative humidity can lie between ice saturation and water saturation for these flights and is not confined to ice saturation only. Clear air values appear to lie close to ice saturation but are generally subsaturated.

The large dispersion in the relative humidity data should be borne in mind when inspecting fig 4. Figure 4 [left] shows SID spherical fraction, that is the fraction of particles in 1-s that have $Af < 12$, versus relative humidity. Choosing different Af thresholds has the effect of moving the data along the spherical fraction axis, but does not affect the qualitative distribution of the data. This plot shows a distinct separation in the data. For SID spherical fractions greater than 0.7 the nominal relative humidity is close to 1 (water saturation). For spherical fractions less than 0.3 a wide range of nominal relative humidity from 0.7 to in excess of 1.1 is seen. There are very few 1s intervals exhibiting spherical fractions between 0.3 and 0.7. Small liquid droplets that are detected by the SID probe (diameter $< 35\mu$m) rapidly evaporate when the relative humidity falls below

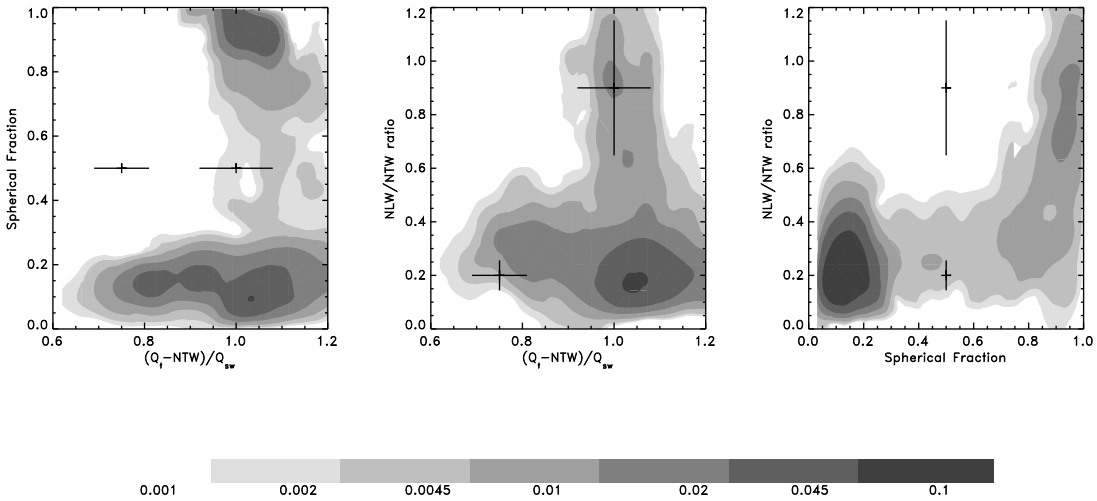

Figure 4. [left] SID spherical fraction against relative humidity. [middle] Nevzorov liquid and total condensed water ratio against relative humidity. [right] Nevzorov liquid and total condensed water ratio against SID spherical fraction. The contours represent the bin normalised concentration: (number in bin)/(N), where for [left] N=8052, dx=0.04, dy=0.07; [middle] N=7917, dx=0.04, dy=0.10; [right] N=8034, dx=0.06, dy=0.10. Bin widths, dx and dy, have been chosen throughout to ensure a similar dynamic range for these and subsequent contour plots. These plots are derived from 1-s data where NTW>0.01 g kg^{-1} and SID concentration > 0.2 cm^{-3}. Examples of 1 standard deviation are given in each plot.

water saturation and so the confinement of high spherical fractions at humidities at or close to water saturation suggests that using the particles sphericity is a good proxy for the phase of the particle, that is, when a particle is determined to be spherical by the SID it is liquid. The excess nominal relative humidity values observed when ice is present are greater than those seen for liquid only and expected from the combination of individual measurement errors. This suggests either that Q_t is over estimated when ice is present or that NTW is underestimating the total condensed water content, or both. The former effects may result from spikes caused by evaporation of individual ice crystals in the total water sensor being outside the range of the calibration. The latter may result from a reduced collection efficiencies of the NTW for larger ice crystals.

A similar plot using the ratio of the uncorrected NLW sensor to the NTW sensor versus nominal relative humidity is shown in fig. 4 [middle]. In this figure high NLW/NTW ratios have a nominal relative humidity around 1. High NLW/NTW ratios, that can exceed 1, merge into lower values that spread over a wide relative humidity range. Unlike the spherical fraction plot there are no discrete islands of data. Because of random error and the fact that NTW and NLW have different collection efficiencies as a function of particle size the ratio of NLW/NTW can exceed a value of 1.0 (see Strapp et al. 2003). Given the random error of 20% for each of the NLW and NTW, we expect the ratio NLW/NTW to have an error of 28%.

Plotting the NLW/NTW ratio against the spherical fraction (fig 4 [right]) gives a clustering of data points with low spherical fractions and low NLW/NTW ratios. The mean NLW/NTW ratio for low spherical fractions is ~0.2, indicating that the NLW responds to ice particles as Korolev et al. (2003) suggest. A value of 0.2 is higher than the 0.11 reported by Korolev et al. (2003). Possible reasons may be related to the air-

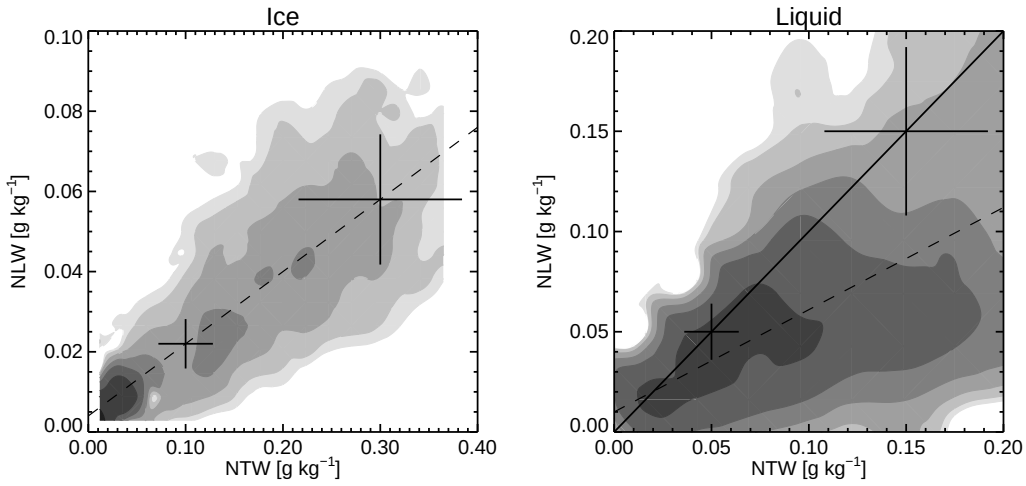

Figure 5. [left] Nevzorov liquid water values against Nevzorov total condensed water content values in regions determined to be ice by the SID probe. The dashed line was obtained through linear regression: NLW=0.18×NTW (1% error on fitted gradient). [right] Nevzorov liquid water values against Nevzorov total condensed water content valuess in regions determined to be liquid by the SID probe. The dashed line was obtained through linear regression: NLW=0.51×NTW+0.01 (2% error on gradient, 10% error on intercept) The contours (see fig 4 for contour values) represent the bin normalised concentration: (number in bin)/(N), where for [left] N=5291, dx=0.02, dy=0.006; [right] N=2617, dx=0.03, dy=0.03. These plots are derived from 1-s data where NTW>0.01 g kg^{-1} and SID concentration > 0.2 cm^{-3}. Examples of 1 standard deviation are given in each plot.

speed used for sampling (typically ∼120 m s^{-1}) and the location of the sensor. For high spherical fractions (> 0.7) the NLW/NTW ratio can be as low as 0.2. 1s regions where 0.4<spherical fraction<0.85 and 0<NLW/NTW ratio<0.45 are probably regions where ice and liquid are coexisting within a 100m interval in the SID size range. We shall see later that when SID is dominated by liquid there may still be larger ice present.

Using 1-s periods when the SID probe determines that ice number concentration is dominant we can look at the response of the NLW sensor to ice. Figure 5 [left] shows that on average the NLW sensor detects a value of 0.18 of the value detected by the NTW sensor using 1-s data. When 1-s periods containing some liquid as indicated by the SID are used the contours follow the 1:1 line but are also affected by mixed-phase regions that lead to increased NTW relative to NLW (fig. 5 [right]).

We can derive an independent measure of IWC from using the Total Water Content probe (IWC$_{Q_t}$). This instrument completely evaporates hydrometeors as they enter the probe and then measures the total water content (vapour + condensed) by means of Lyman-alpha absorption with sampling carried out at 64 Hz. Nicholls et al. (1989) showed that individual hydrometeors produce a spike with an exponentially decaying tail in the Q_t signal. The 'high' frequency spikes caused by particles are superimposed on the 'lower' frequency vapour signal. If the spikes are discrete as they tend to be in ice conditions, then by fitting a 'low' frequency (10 Hz) line at the base of the spikes gives an estimate of the water vapour content. For each second the water vapour estimate can be removed from the Q_t signal to give an estimate of the ice water content (see Wood and Field 2000). In liquid conditions, the numbers of particles encountered is so large that the spikes merge and the line fitted to the base of the spikes will include a contribution from

the condensed water. Therefore, in mixed-phase conditions the estimated condensed water content will be underestimated if LWC dominates the total condensed water content. Here we compare the 1 Hz response of the NTW and Total Water Content probe estimate of condensed water content (IWC_{Q_t}) from these three flights. Fig 6 [left] shows a plot of NTW against IWC_{Q_t} where two groupings of data can be seen. One grouping is close to a 1:1 line whereas the second grouping shows an underestimate of condensed water relative to the NTW. The grey shading reveals that the approximately 1:1 grouping is found where SID indicates a dominance of ice (light grey points) and the other grouping is located in regions determined as being liquid dominated by SID (dark grey points). The black points are regions where SID determined that the dominant phase was liquid (in the small particle size range) and large 2D-C particles were detected (diameter>200 μm and concentration > 1 m^{-3}): possibly mixed-phase regions. The location of possible mixed-phase points amongst the ice indicates that the majority of the mass is located in the ice particles. There is a subset of possible mixed-phase points that are found amongst the liquid dominated points when the FSSP and SID indicate concentrations of 10s cm^{-3}. On inspection of 2D-C images associated with these points we found that in some cases large circular particles (300-400 μm in diameter) were present that may be large supercooled drizzle drops. In the supercooled stratocumulus case (28th February 2001) it appeared that only low concentrations of large ice crystals with dendritic features were present and so the condensed water content was dominated by the LWC. The plot of NTW against IWC_{Q_t} also shows that for low NTW values the value of IWC_{Q_t} can be several time larger than NTW. This is most likely due to size of the baseline smoothing window (10 Hz) used to remove the contribution of the vapour from the 64 Hz Q_t signal and will result in IWC_{Q_t}/NTW ratios greater than 1 seen in the rest of fig. 6.

A plot of the spherical fraction versus the IWC_{Q_t}/NTW ratio (fig 6 [middle]) shows a progression from ice with low spherical fractions and 1:1 $\Delta IWC_{Q_t}/\Delta NTW$ ratio, through mixed-phase with higher spherical fractions and 1:1 $\Delta IWC_{Q_t}/\Delta NTW$ ratio to liquid with spherical fractions close to 1 but low IWC_{Q_t}/NTW ratio. A plot of the NLW/NTW ratio versus IWC_{Q_t}/NTW ratio (fig 6 [right]) shows that the liquid and ice dominated regions are seperated into discrete zones. This property can be used practically to diagnose the dominant mass weighted phase independently of the SID probe. As previously mentioned, the ratios greater than 1 are the result of instrumental effects.

The SID determination of the dominant phase in the sub-50μm range is largely consistent with the known or expected response of the Nevzorov and TWC probes. Therefore, we will utilise a combination of the SID definition of phase and the response of the Nevzorov and Total Water Content probes in the following section. It should always be borne in mind that the SID determines the number weighted dominant phase for a 1-s interval (100m) in the sub-$\sim$50μm size range and even when SID detects liquid, large ice crystals detectable by the 2D-C or the IWC_{Q_t}/NTW ratio (presented in fig 6) could also be present making the interval 'mixed-phase'.

We will propose the following conditions for phase determination for each 1-s ($\sim$100m) interval where the SID concentration $\geq$0.2 cm^{-3}. Based on the fact that the SID is dominated by the small particles and the ratio of IWC_{Q_t}/NTW is dominated by the larger particles.

- Ice: SID determines ice dominates in SID size range.
- Liquid: SID determines liquid dominates in SID size range AND NTW>0.01 g kg^{-1}

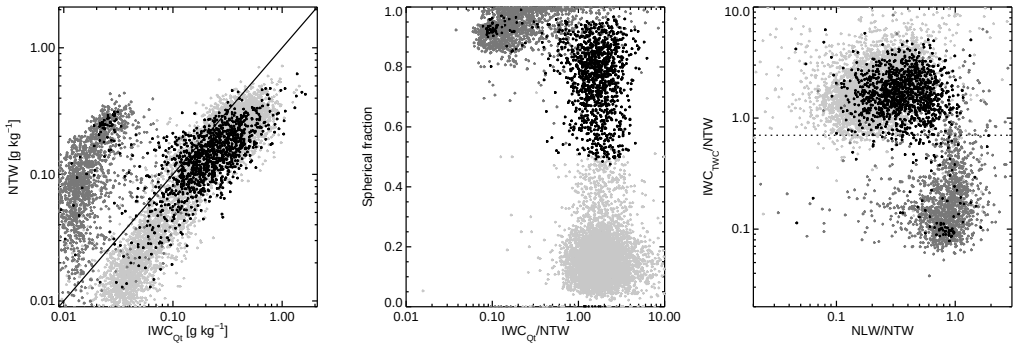

Figure 6. a) Nevzorov total water versus IWC derived from the Total Water Probe. b) SID spherical fraction versus the ratio of IWC derived from the Total Water probe and NTW. Light grey points represent 1-s regions determined to be ice by SID, dark grey points represent liquid, and black points represent regions where SID indicated liquid but the 2D-C recorded particles larger than 200 μm in diameter with a concentration in excess of 1 m^{-3}. c) ratio of IWC derived from the Total Water probe and NTW versus the ratio of NLW and NTW. These plots are derived from 1-s data.

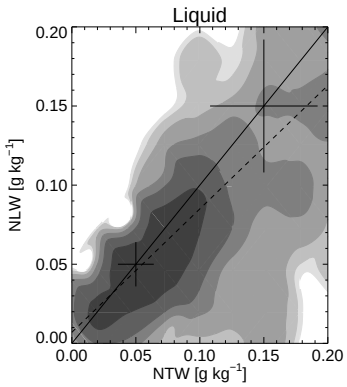

Figure 7. Nevzorov liquid water values against Nevzorov total condensed water content values in regions determined to be liquid only using the definitions given in section 5. The dashed line was obtained through linear regression: NLW=0.78×NTW+0.01 (1% error in fitted gradient, 20% error in fitted intercept). The contours (see fig 4 for contour values) represent the bin normalised concentration: (number in bin)/(N), where N=1392, dx=0.03, dy=0.03. These plots are derived from 1-s data where NTW>0.01 g kg^{-1} and SID concentration $>$ 0.2 cm^{-3}. Examples of 1 standard deviation are given in each plot.

AND IWC$_{Q_t}$/NTW $\leq$ 0.7.

- Mixed-phase: SID determines liquid dominates in SID size range AND NTW>0.01 g kg^{-1} AND IWC$_{Q_t}$/NTW $>$ 0.7.

Using these definitions for the phase of each 1-s interval we can return to the comparison of the NTW and NLW sensors for liquid only regions. Figure 7 shows improved agreement between the probes relative to fig. 5 with the gradient in fig. 7 closer to 1 suggesting that the ice and mixed-phase regions have successfully been filtered out.

We have examined the number weighted mean size of 2D-C particles (D>100μm) for liquid, ice and mixed-phase 1-s periods (fig.8) and see that for ice and mixed-phase the mean size is usually in excess of 200μm whereas for liquid the mean particle size is usually less than 150 μm. This is as expected if the 2D-C particles are ice for ice and mixed conditions and drizzle droplets in liquid conditions. It is also notable that the fraction of

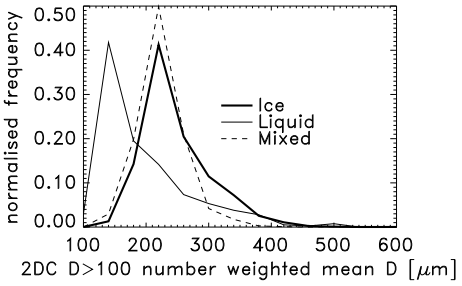

Figure 8. Frequency plots of the number weighted mean particle diameter from the 2D-C probe for ice, liquid and mixed-phase conditions.

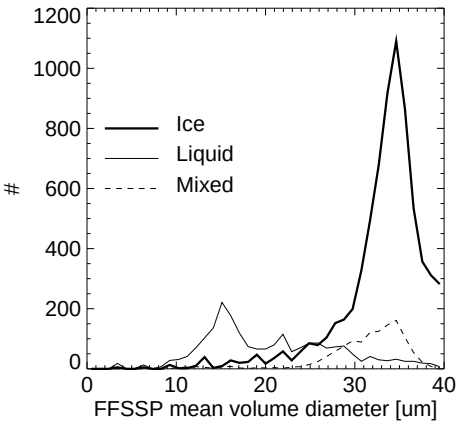

Figure 9. Mean volume diameter (1 Hz values) from the FSSP assuming all particles are spherical for conditions when liquid only (thin solid), ice only (thick solid) and mixed (dashed) conditions are observed.

1-s periods for ice, liquid and mixed-phase that have 2D-C concentrations greater than 1 m^{-3} for particles larger than 200 μm are 0.75, 0.16 and 0.94, respectively. The relatively low frequency of occurrence of large 2D-C particles is what would be expected for super cooled drizzle conditions.

Finally, Cober et al. (2001) showed that in ice conditions the median volume diameter (ratio of 4th and 3rd moments of diameter) of the FSSP size distribution displayed a value of $\sim$>30 μm when ice crystals were present in contrast to $\sim$10μm for purely liquid conditions. Using the phase determination of dominant phase that is presented above we histogrammed the mean volume diameter for $\sim$100 m regions containing liquid only, ice only or mixed-phase (fig. 9). It can be seen that the liquid only mean volume diameter is $\sim$10μm, but the mixed-phase and ice only regions both show peaks at $\sim$30μm, in agreement with Cober et al. (2001), and supporting our phase definitions.

6. Radar-aircraft observations

Here we highlight one run from each flight that exhibits interesting characteristics and show it in the context of the radar observations. The radar imagery with the phase indication defined above provides the best overview. It is known that the Nevzorov liquid water sensor has a residual signal in ice. No attempt at removing that effect has been

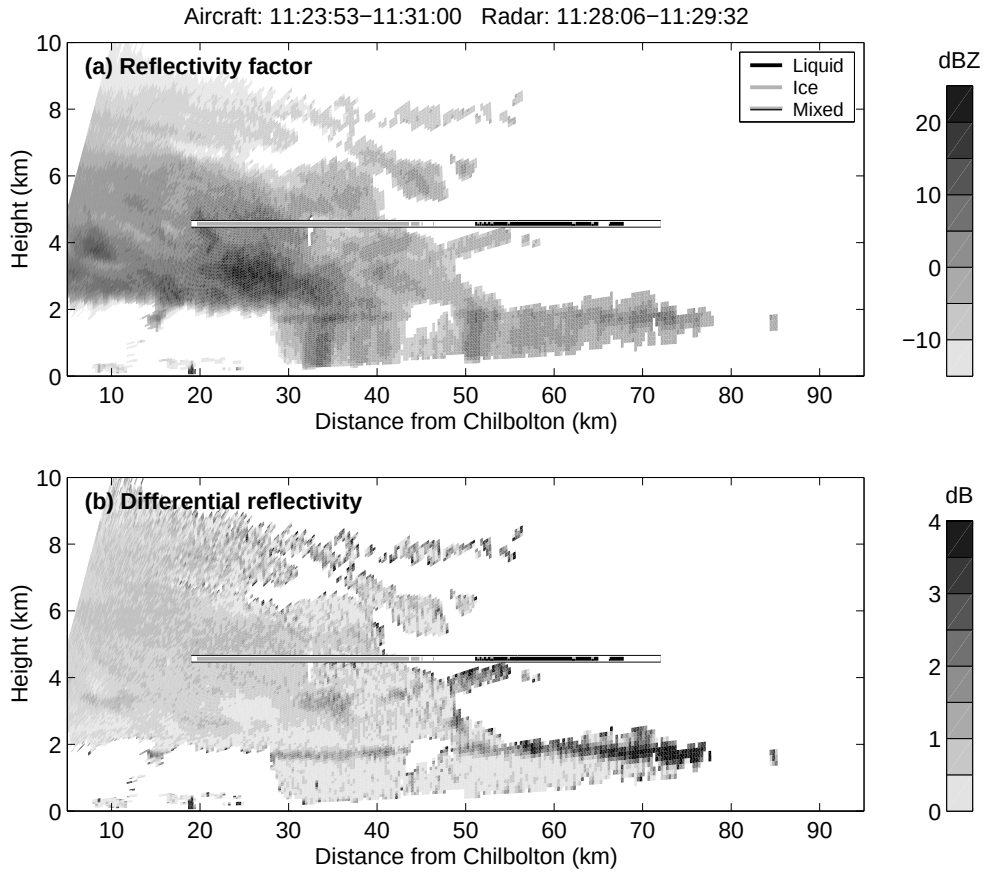

Figure 10. Simultaneous aircraft and radar data obtained at 1130 20th October 2000. The top panel shows radar reflectivity and the bottom panel shows differential reflectivity for the same scan. The horizontal line at 4 km is the aircraft run at -13.5C. The dark region indicates where the SID determined the phase to be ice and the light region is where the SID determined the phase to be liquid. A region with light on the top and dark on the bottom is a mixed-phase region.

made for the following composite figures.

On the 20th October 2000 (A803 Run 2.2) during the middle part of the flight the radar showed the rear end of the frontal cloud to have some trailing thin layered cloud (fig 10). The flight leg carried out at 4 km (-13.5C) started at a range of 75 km in mainly liquid conditions with droplet concentrations indicated by the FSSP and SID as $\sim$10 cm^{-3} (fig. 11). There was some indication of large dendritic ice shown on the 2D-P at very low concentrations ($\sim$60km, not shown). In this region the vapour mixing ratio estimated from the TWC and Nevzorov probe was close to water saturation. The Nevzorov liquid and total condensed water sensors showed consistent values but sometimes had 1s ratios as low as 0.3. The radar data showed high ZDR values and low reflectivities in this layer cloud region just below the flight level (range 50-60 km). The minimum detectable reflectivity signal by the radar at this range was -7 dBZ and therefore was unable to detect small droplets at this range. Between 50 to 45 km there were not many

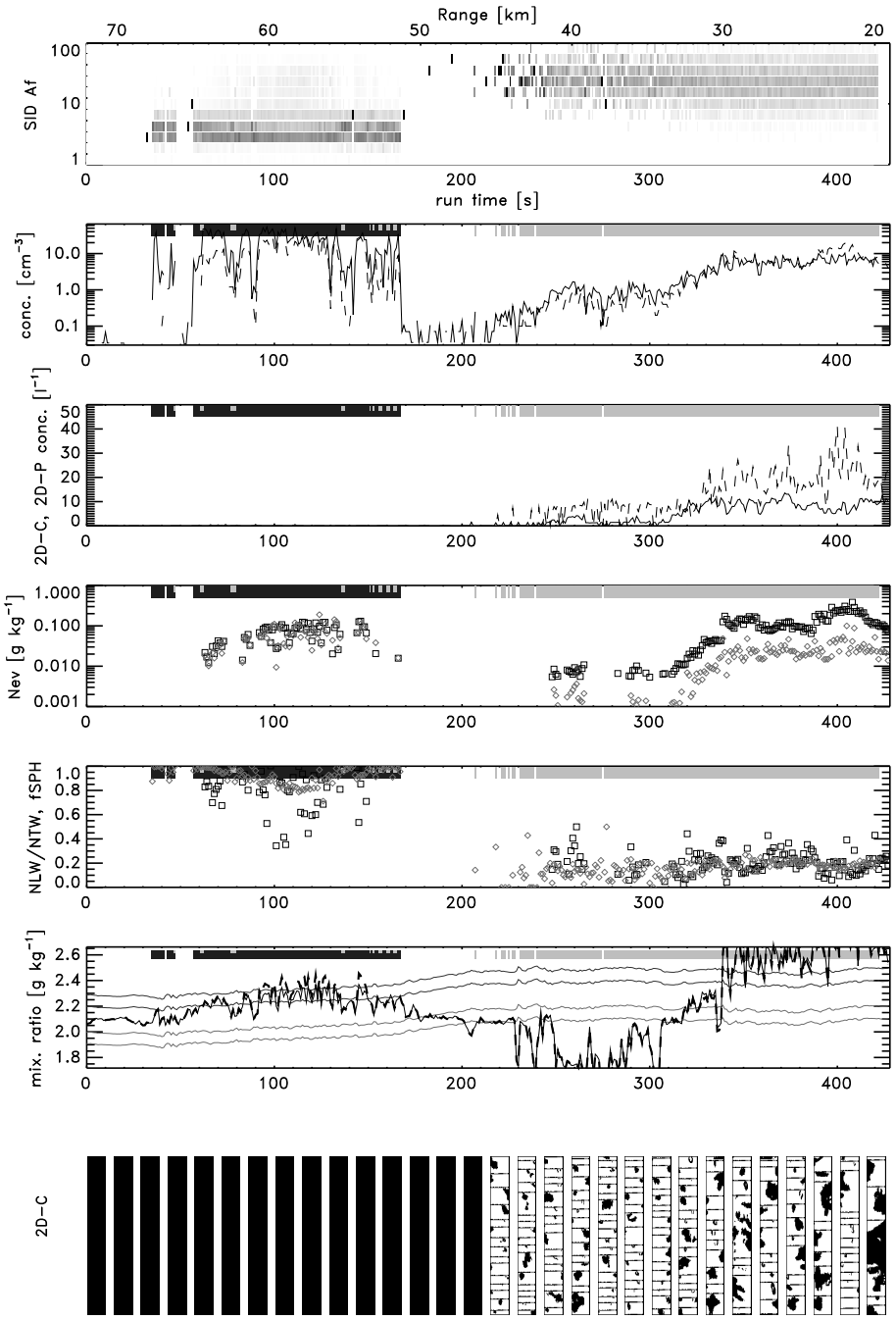

Figure 11. The composite figures show various parameters as a function of run time (s) and range from the radar. The two-tone grey bar at the top of the panels represents the dominant phase as determined from the SID probe: dark grey is for liquid, light grey is for ice and background white means that fewer than 5 particles were observed in a 1s interval and so no determination was made. Mixed-phase regions are where both grey shades are present in the same 1s period. The panels from top to bottom show: (i) SID Af values binned in 1s and logarithmic Af bins - the grey shade repesents the 1-s concentration in each Af bin with darkest having the highest concentrations; (ii) 1 Hz SID concentration (solid) and 1 Hz FFSSP concentration (dashed) [cm^{-3}]; (iii) 1 Hz 2D-C concentration (dashed) for maximum dimension >100μm [l^{-1}] and 1 Hz 2D-P concentration (solid) for maximum dimension >200μm [l^{-1}]; (iv) 1Hz Nevzorov total condensed water (black squares) and Nevzorov liquid water (grey diamonds) [g kg^{-1}]; (v) 1 Hz SID spherical fraction ($N_{Af<12}/N$, diamonds) and the NLW/NTW ratio (squares). Both of these values should be 1 in liquid cloud; (vi) 1 Hz Water vapour mixing ratio. The upper pair of darker grey lines show the values for water saturation using the run pressure and temperature ±0.25C. The lower pair of lighter grey lines show the values for ice saturation. The solid black line shows the vapour mixing ratio derived from Q_t - NTW. The dashed line shows the mixing ratio derived from Q_t-IWC$_{Q_t}$, where IWC$_{Q_t}$ is estimated from the total water probe; (vii) Example 2D-C imagery alligned with the run time. The width of each bar is 800 μm.

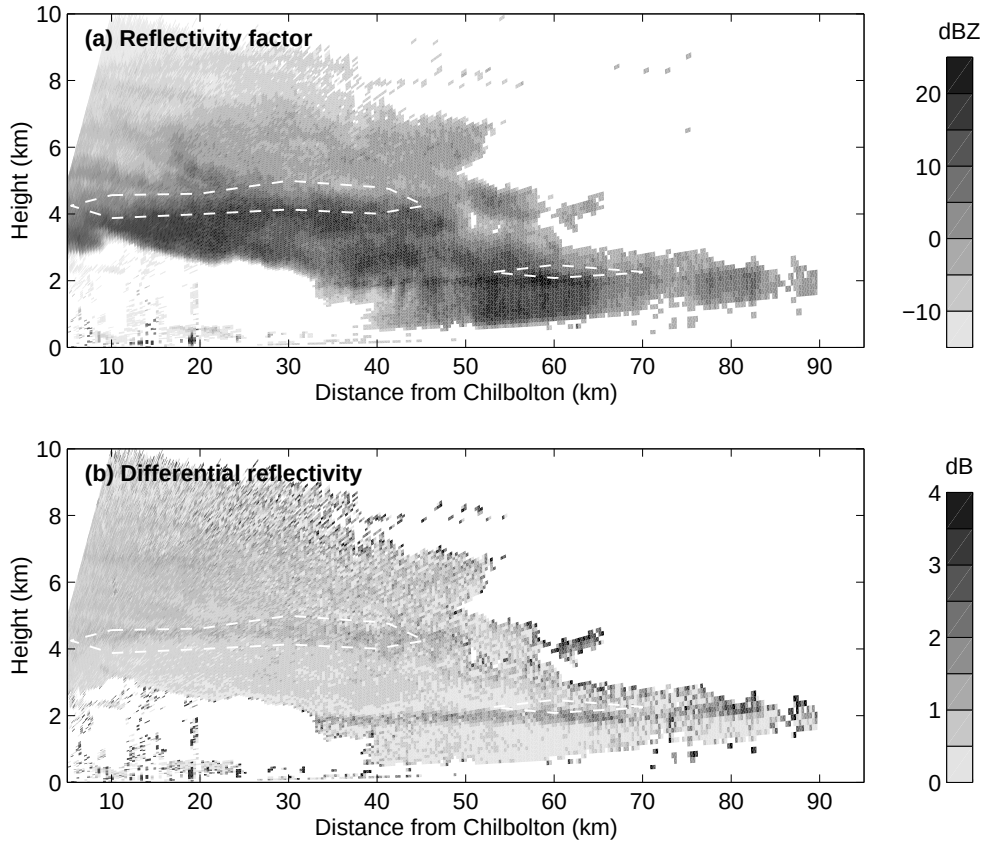

Figure 12. Same as fig 10 but slightly earlier on the 20th October 2000. The white dashed contour indicates where the vertical gradient in reflectivity falls below -10 dBZ/km. This region marks a rapid growth in ice mass at 4.5 km and the melting layer at 2 km.

particles encountered. As the aircraft moved closer than 45 km the SID indicated ice cloud particles increasing in concentration as did the 2D probes. 2D-C imagery showed that the ice particles at a range of less than 45 km were not pristine and that the ZDR values were low. The NLW/NTW ratio was generally around 0.2. It is notable that the ZDR signal in the melting layer at 60-70 km range is above 7dB indicating that oblate (pristine) ice particles that have presumably fallen from the thin cloud layer above are melting and becoming detectable by the radar.

The radiosonde (Vaisala RS80) ascent from Larkhill (25 km to the west of Chilbolton) at 10 UTC indicated relative humidities with respect to water of 96% between -10 and -20degC. Given the likely error in the sonde measurement of 5% and the fact that a radiosonde gives a point measurement it appears that the air was close to liquid saturation at this height, so a likely explanation for these observations is that there was a tendency for supercooled liquid water to form at the altitude of the aircraft in Fig. 8. Beyond 50 km from Chilbolton, the liquid was measured by the aircraft and the small amounts of ice detected by the radar at this altitude had elevated values of ZDR, indicating pristine growth of ice crystals with high axial ratios and high ice supersaturations. At closer ranges to the radar the ice falling into the layer depleted the liquid via accretion and

to a lesser extent the Bergeron-Findeisen mechanism and only ice was measured by the aircraft. It is interesting that in the scans taken in the 30 minutes leading up to the scan shown in Fig. 8, a strong increase in radar reflectivity was observed as the ice fell through the 4-4.5 km altitude range. Fig 12 shows the radar data from 11:08 UTC, at which time the aircraft was unfortunately not flying in cloud. The white dashed contour indicates where the vertical gradient in reflectivity falls below -10 dBZ/km. This was calculated from reflectivity degraded to 10 km in the horizontal and 0.5 km in the vertical. A clear layer of high vertical reflectivity gradient is evident out to 40 km. This suggests that a layer of liquid water was present here and that it was promoting the rapid growth of ice via riming and vapour deposition, but that it was depleted by the time the aircraft came to sample at this altitude in Fig. 8. The ZDR was not especially large where this increase in refectivity was occurring, presumably because the ice particles falling into the layer were mostly low-density aggregates, and the enhanced growth could not promote more planar or columnar forms.

We have not included timeseries of vertical wind velocity as we do not see any consistent correlations between phase structure and vertical wind structure during these flights. This is to be expected by the unstable nature of mixed-phase conditions. Because updraught and downdraughts are observed at random times relative to their origin the complex production and loss of droplets and ice crystals within a cloud volume can be at various stages from totally liquid to completely glaciated. However, Korolev and Mazin (2003) propose the existence of an interesting equilibrium state where a constant updraft can maintain a mixed-phase cloud. The magnitude of the minimum updraft required increases as a power law function of the 'integrated ice particle radius' (ice concentration $\times$ mean ice particle size). Unfortunately the accuracy of the vertical wind measurements during these flights precludes testing of this assertion.

On the 21st November 2000 (A806, fig 13) a flight was made in frontal cloud that had increasingly more active embedded convection present. By comparing consecutive runs (Run 4 – Run 7) an evolving cumuliform structure was revealed in the reflectivity signal between 3-5 km in altitude that moves towards the radar. No significant accompanying structure was seen in the ZDR signal. The SID probe showed regions of liquid domination (in the small particle range) along the run that were not related to any obvious structures in the reflectivity. This included regions that were outside of the obvious plume structure (e.g. fig 14, 40-50km, Run 6, T=-8C). The regions where the SID indicated a dominance of liquid water also contained larger ice particles indicating mixed-phase conditions along this run. This run displayed the complicated interleaved structure that these mixed-phase clouds can have with numerous 100-m-scale , or so, liquid intrusion into the surrounding ice cloud. It is noteworthy that the low reflectivity region in fig. 12d (range 40 km) was coincident with the presence of liquid. The persistence of the liquid was presumably due to the low loss rate of liquid to ice through accretion and to a lesser extent the Bergeron-Findeisen process because of the relatively low mass density of ice present.

As with the 20th October 2000 case, the ice had fallen some 4 km before it encountered the liquid water at the altitude of the aircraft. The ice was presumably aggregated so the ZDR remained low. The much more intermittent nature of the liquid water distribution, presumably due to the more convective nature of the cloud, then meant that an associated strong vertical reflectivity gradient did not occur. The presence of a plume visible in the reflectivity is similar to that reported by Hogan et al. (2002), but a major

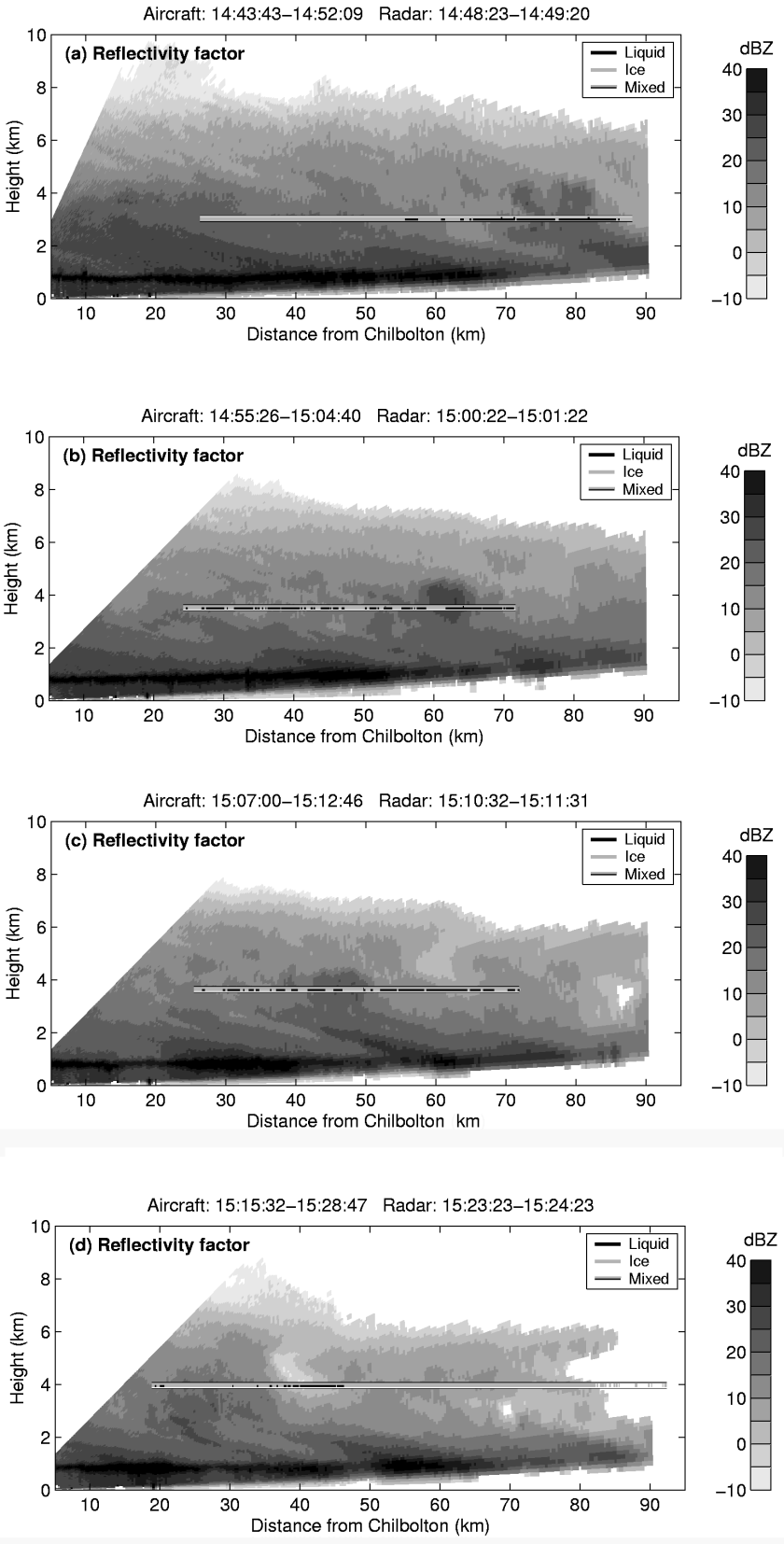

Figure 13. Simultaneous aircraft and radar data from 21st November 2000. The four panels show radar reflectivities from a series of scans. The horizontal line at 4 km is the aircraft run at -8C.

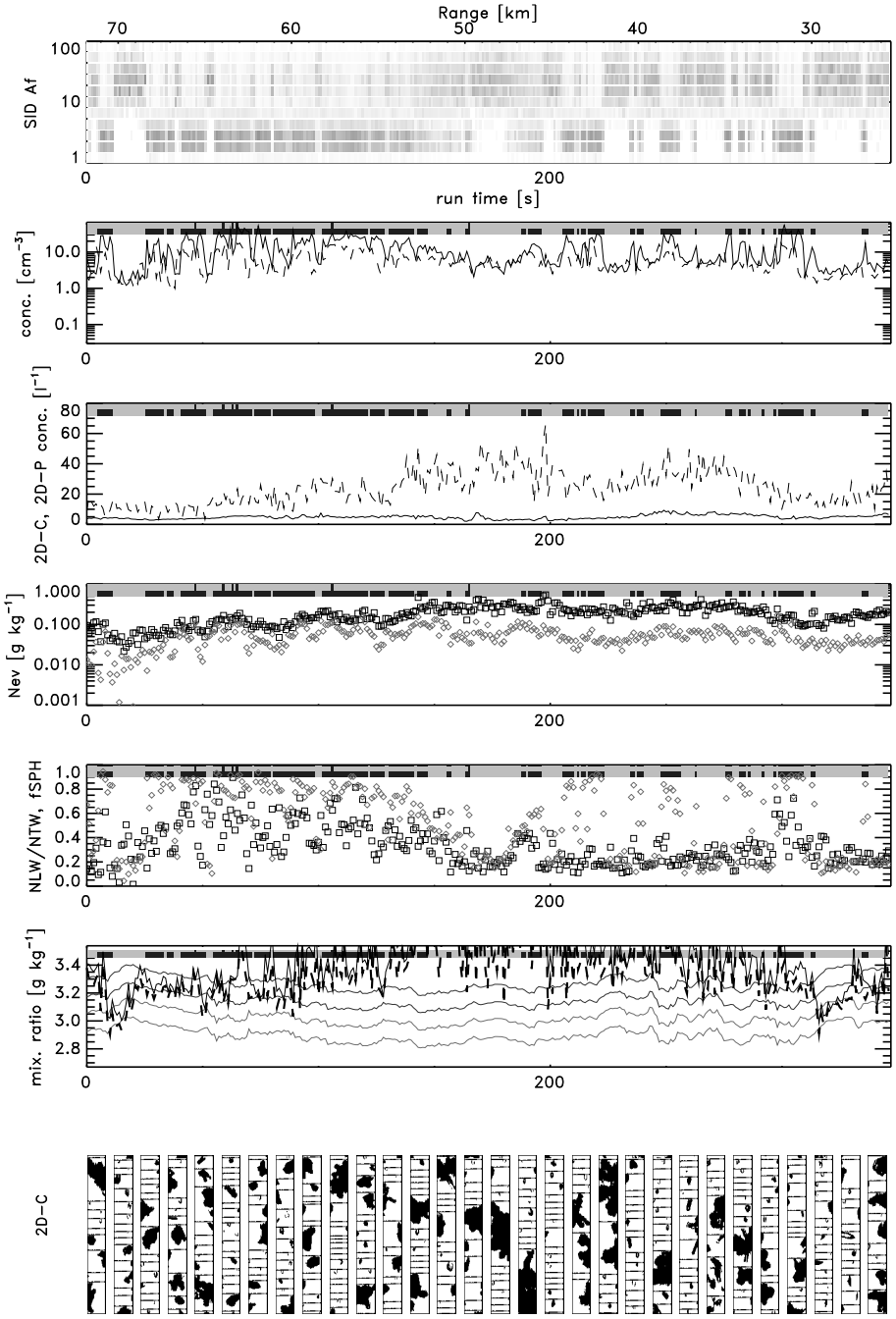

Figure 14. same as figure 11 but for Run 6 21st November 2000.

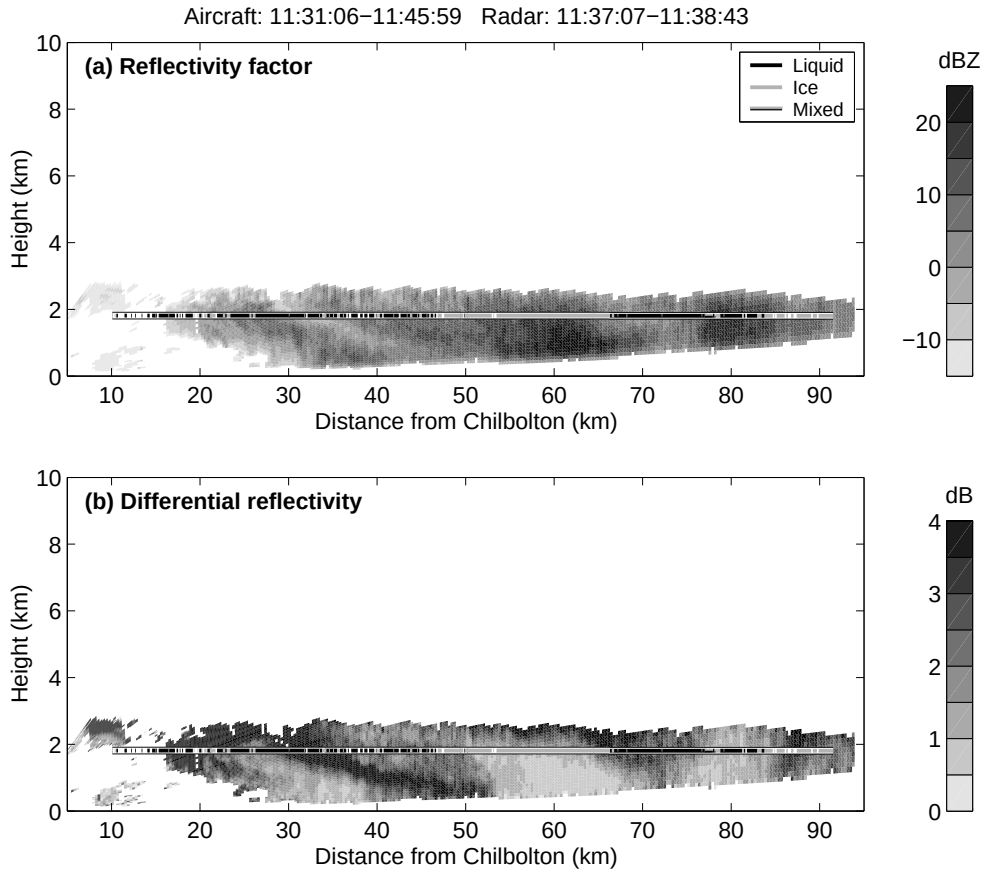

Figure 15. same as fig. 10 but for 28th February 2001.

difference between that case and this is that there was no strong accompanying ZDR signal.

The flight on the 28th February 2001 (A819, fig 15) was made in supercooled stratocumulus. The ZDR signal for Run 1 was much higher then in previous cases, in places reaching 8 dB, and exhibited structure on the scale of 10 km that was anticorrelated with the reflectivity. The flight level of the aircraft at this time was just below 2km (T=-8C). The SID phase determination showed liquid colocated with the high ZDR regions for this run although the situation was not so clear for other runs during this flight (fig 16). Imagery from the 2D-C probe shows well developed dendritic features throughout the middle portion of the run. Between 500-600s along the run the SID indicates that the particles were mostly spherical. However, the concentrations were low and the estimated relative humidity was close to ice saturation. This is a good example of where quasi-spherical ice particles have been present and misinterpreted by the SID as liquid.

The reason for the much higher ZDR in this case compared to the first two cases is that this cloud was mixed-phase all the way to cloud top and entirely within the

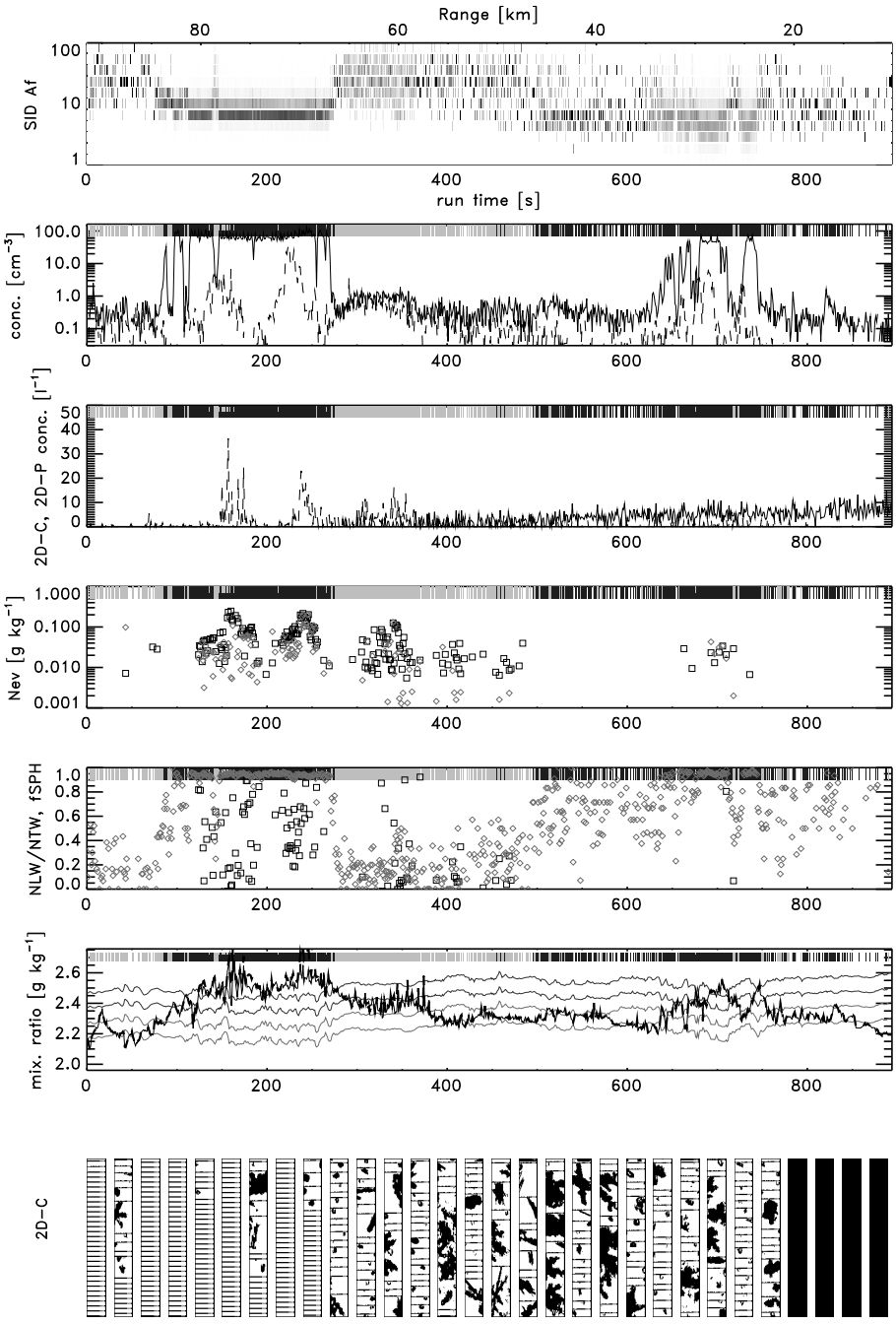

Figure 16. same as fig. 11, but for Run 1 28th February 2001.

planar and columnar growth temperature range whereas the other cases produced well developed aggregates. In this case vapour deposition dominated over aggregation throughout the crystal lifetime, resulting in large pristine dendrites with extreme aspect ratios. Nonetheless, aggregation was presumably important in the higher reflectivity area of the cloud centred at 60 and 80 km from Chilbolton, where the ZDR was much lower. As with the 21 November 2000 case, and indeed as would be expected for stratocumulus, this cloud was rather convective in nature. This is demonstrated by the intermittent nature of the SID liquid water trace, but also the estimated vertical wind velocities measured by the vertically pointing 94-GHz cloud radar at Chilbolton (not shown), which were fluctuating quite strongly with an amplitude of around 0.5 m/s, on the scale of a few minutes as the cloud was advected over the site.

7. Discussion

It can be seen from these comparisons of radar and aircraft data that the structure of the mixed-phase regions is very complex. A number of previous studies have suggested that layered mixed-phase clouds are formed of predominantly liquid phase near cloud top and ice phase lower down (Fleishauer et al. 2002, Pinto et al. 2001, Hogan et al. 2003a) in qualitative agreement with the observations in the Ac layer from the first flight. However, the frequent pulses of liquid embedded in ice cloud extending for $\sim$100s metres illustrated in the 21st Novemeber 2000 case is also documented for other clouds by Lawson et al. (2001) and Korolev et al. (2003). It appears that there are two 'modes' for super cooled liquid water. In the first more stable mode, the supercooled water is found in a horizontally continuous (kilometres) mantle on top of relatively thin layered cloud. It is thought that the liquid water layer serves as a production zone for the ice, forming the ice cloud below. In the second more transient mode, the intermittent pulses on small scales of 100s metres in the horizontal and presumably relatively short temporal scales are produced and destroyed through the competing effects of turbulence and uplift, for example (liquid production), and coexistence with large ice crystals (liquid loss via accretion and vapour deposition). The main difference between these two modes that leads to their different manifestations is the relative size of the loss rate to the production rate. When the large amounts of ice are present liquid droplets are rapidly removed as was seen in the 21st November 2000 case. But when large amount of ice are not present, and mixing with dry air or subsidence is not driving evaporation, then liquid droplets can persist as was seen in the 20th October 2000 case.

The lack of variation in the ZDR signal for the 21st November 2000 case, despite the presence of liquid water, suggests that the morphology of the ice crystals sedimenting from above was not sufficiently modified by high humidities associated with the liquid water. Thus, sedimenting aggregates can mask the presence of supercooled water as far as the radar is concerned. Therefore, when aggregation dominates the morphology of the crystal, the ZDR signal is low and when diffusional growth dominates the crystal morphology the ZDR signal can be high if crystals with high axial ratios are produced (planar or columnar growth).

Using the definitions of liquid, ice and mixed-phase from section 5 we have tabulated (table 1) and plotted (fig 17) the frequency of ice, liquid and mixed-phase 1-s ($\sim$100 m) intervals as a function of temperature. Additionally, following Korolev et al. (2003) and assuming the residual effect of ice on the NLW is 0.18 we have computed

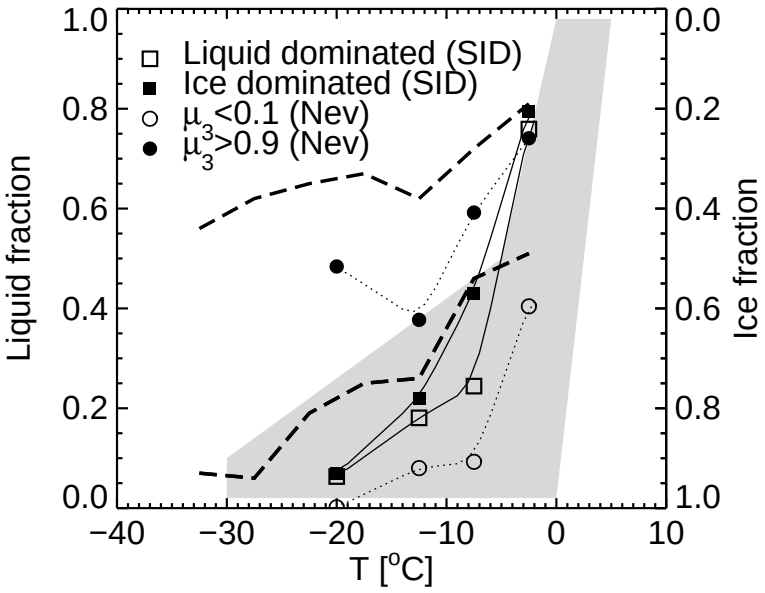

Figure 17. Plot of liquid and ice fraction versus temperature. The shaded region marks the approximate region occupied by 2-minute averages of lwc/(iwc+lwc) from Moss and Johnson (1994) and Bower et al. (1996). The dashed lines mark the fraction of cloud encountered with $\mu_3 < 0.1$ (liquid fraction, lower line) and when $\mu_3 > 0.9$ (ice fraction, upper line) from Korolev et al. (2003). The symbols are average values for four temperature ranges: 0C– -5C, -5C– -10C, -10C– -15C, -15C– -25C. The SID data are for 1-s intervals with concentrations >0.2 cm^{-3}. The Korolev et al. data are for 1-s intervals with NTW>0.01 g kg^{-1}.

μ_3 (=IWC/(IWC+LWC)) for all 1-s intervals with NTW>0.01 g kg^{-1}. From the SID-Nevzorov-TWC probe response it is notable that the fraction of mixed-phase intervals is approximately equal to the fraction of liquid only intervals in the -5C to -10C temperature range. For the other temperature ranges the mixed-phase regions are typically much less frequent than the liquid only intervals. The Hallett-Mossop process is potentially active as a source of ice particles within liquid containing clouds in this temperature range. The similarity of liquid and mixed-phase fractions may therefore be indirect evidence of the Hallett-Mossop processes activity. However we would expect to increase the number of data samples in other temperature ranges to a comparably high value before commenting further on this. Overall, the fraction of mixed-phase regions for these flights is about half the fraction of liquid only regions. In contrast the mixed-phase fraction (fraction of μ_3 for which $0.9 > \mu_3 > 0.1$) from the Nevzorov probe alone is roughly constant and exceeds the liquid fraction for temperatures colder than -5C. The SID-Nevzorov-TWC diagnosed phase indicates that most 100 m regions are either ice or liquid only, whereas the Nevzorov indicates a much larger propotion of mixed-phase regions.Korolev et al. show higher fractions of liquid water, slightly lower ice fractions and roughly constant mixed-phase fractions at all temperatures. These differences could arise from the different datasets used.

The mass weighted datapoints obtained by Bower et al. (1996) and Moss and Johnson (1994) are contained within the shaded region (fig. 17) but tend to be concentrated towards the lower liquid fraction and warmer temperature extremes of the indicated envelope. The clouds sampled by Bower et al. 'were mostly of frontal origin. It should also

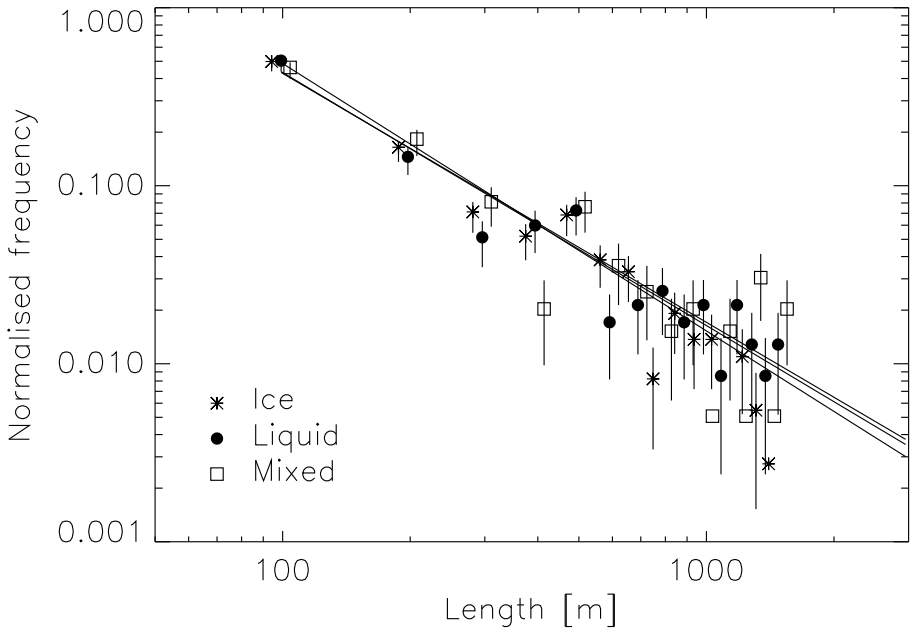

Figure 18. Normalised histograms of contiguous cloud segment lengths from the three flights presented in this paper. The ice, liquid and mixed phase points are represented by asterisks, circles, and squares, respectively. The error bars represent the Poissonian counting error. The number of cloud segments used for each phase are 384 for ice, 245 for liquid and 204 for mixed-phase.

be noted that phase detection method utilised a 2D-C probe and a liquid water hotwire sensor and so there were uncertainties in the identification of sub-100μm particles.

We have pointed out that liquid water intrusion into surrounding ice cloud can appear on scales as small as 100 m. It is interesting to plot histograms of the contiguous lengths of liquid, ice and mixed phase clouds encountered for the three flights using the phase definitions given in section 5. Figure 18 shows the normalised frequencies and the weighted least squares fit lines. The histograms of cloud segments lengths for the different phases follow power law relationships. The gradients are found to have values of -1.5, -1.4, -1.4 (all ± 0.4) for ice, liquid and mixed-phase cloud segments lengths, respectively. Similar power laws are obtained when different concentration thresholds are used to decide if a 100m segment is cloudy or clear. This indicates that smaller regions of cloud, whether mixed-phase, liquid or ice, are found more frequently than longer segments.

We have further highlighted the difference between the Nevzorov definition of phase and that given in section 5 by plotting μ_3 as a function of spherical fraction in fig 19 using three sets of contours to represent liquid, ice and mixed-phase regions determined from the definitions given in section 5. It can be seen that a spherical fraction of ~ 0.5 divides the regions into observations of ice only and regions containing some liquid. While the ice only region is located at high values of μ_3 as expected, the liquid and mixed-phase points extend across a wide range of μ_3 values. This illustrates that the definition of the phase within a cloud volume is critical to the values of the statistics obtained. This should be borne in mind when attempting to make comparisons between models and observations.

Table 1. Columns 2-5 contain the frequencies of liquid only, ice only and mixed-phase 1-s intervals and the number of intervals, N, in the temperature using the criteria given in section 5. Columns 6-9 contain the frequencies of liquid only, ice only and mixed-phase 1-s intervals and the number of intervals, N_{nev}, in the temperature obtained from the Nevzorov probe for the criteria: liquid only, $\mu_3 < 0.1$; ice only, $\mu_3 > 0.9$; mixed-phase, $0.1 < \mu_3 < 0.9$ and NTW>0.01 g kg^{-1}..

	SID, IWC_{Qt}/NTW				Nevzorov			
T range C	ice frac	liquid frac	mixed frac	N	ice frac	liquid frac	mixed frac	N_{Nev}
0 to -5	0.21	0.76	0.03	889	0.26	0.40	0.34	193
-5 to -10	0.57	0.24	0.19	5667	0.41	0.09	0.50	4250
-10 to -15	0.78	0.18	0.04	2992	0.62	0.08	0.30	1835
-15 to -25	0.94	0.06	0.00	2673	0.43	0.05	0.52	1874

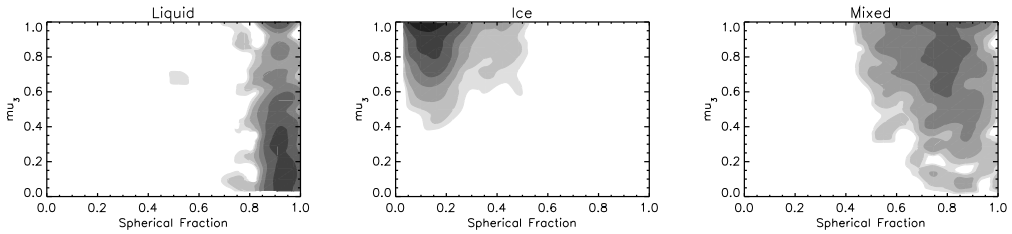

Figure 19. Nevzorov μ_3 versus SID spherical fraction for liquid only [left], ice only [middle] and mixed-phase [right] conditions. The contours (see fig 4 for contour values) represent the bin normalised concentration: (number in bin)/(N), where for [left] N=1054; [middle] N=5440; [right] N=1079 and for all dx=0.06,dy=0.07. These plots are derived from 1-s data where NTW>0.01 g kg^{-1}.

We present 1-s condensed water contents and measured concentrations for liquid and ice regions determind by SID as a function of temperature to show the ranges of values encountered (fig 20). Maximum values of IWC reach 1 g kg^{-1} at -10C and fall to 0.1 g kg^{-1} at -30C [top left]. For liquid water only regions maximum values of LWC are 0.4 g kg^{-1} at -10C falling to 0.1 g kg^{-1} at -20C. Concentrations from SID show that in liquid conditions [bottom right] concentrations can be in the expected range of 10-100s cm^{-3}, but there are also very low concentrations which may be the result of misdiagnosis of the phase by the SID probe. In ice conditions the maximum 1-s concentrations are generally a few per cm^{-3} at all temperatures encountered here. Mixed-phase conditions, on average, show intermediate values relative to the liquid and ice only regions.

Concentrations measured by the SID and FSSP in regions determined to be dominated by ice from the SID probe show that 1-s SID concentrations are generally higher than the FSSP concentrations by a factor of ~2. It has been shown (Field et al. 2003) that in ice conditions the fast FSSP used here detects particles that have interarrival times centred around 10^{-2}s metre scale) and 10^{-4}s (centimetre scale). It has been suggested that shattering of ice crystals on the probe housing may be responsible for the particles with short interarrival times, although this could not be proven. For these flights the fraction of particles with short interarrival times were approximately 0.5 (over 10-s intervals). Therefore, if shattering were occurring then the FSSP measured concentration would be twice the actual concentration. Because the SID inlet is similar in design to the FSSP inlet it may suffer from the same effects.

In liquid conditions the FSSP/SID concentration ratio versus volume radius, determined from the Nevzorov bulk water content and SID concentration, increases from zero for a 5 μm volume radius to 1:1 at 9μm. This behaviour is due to the different sensitivi-

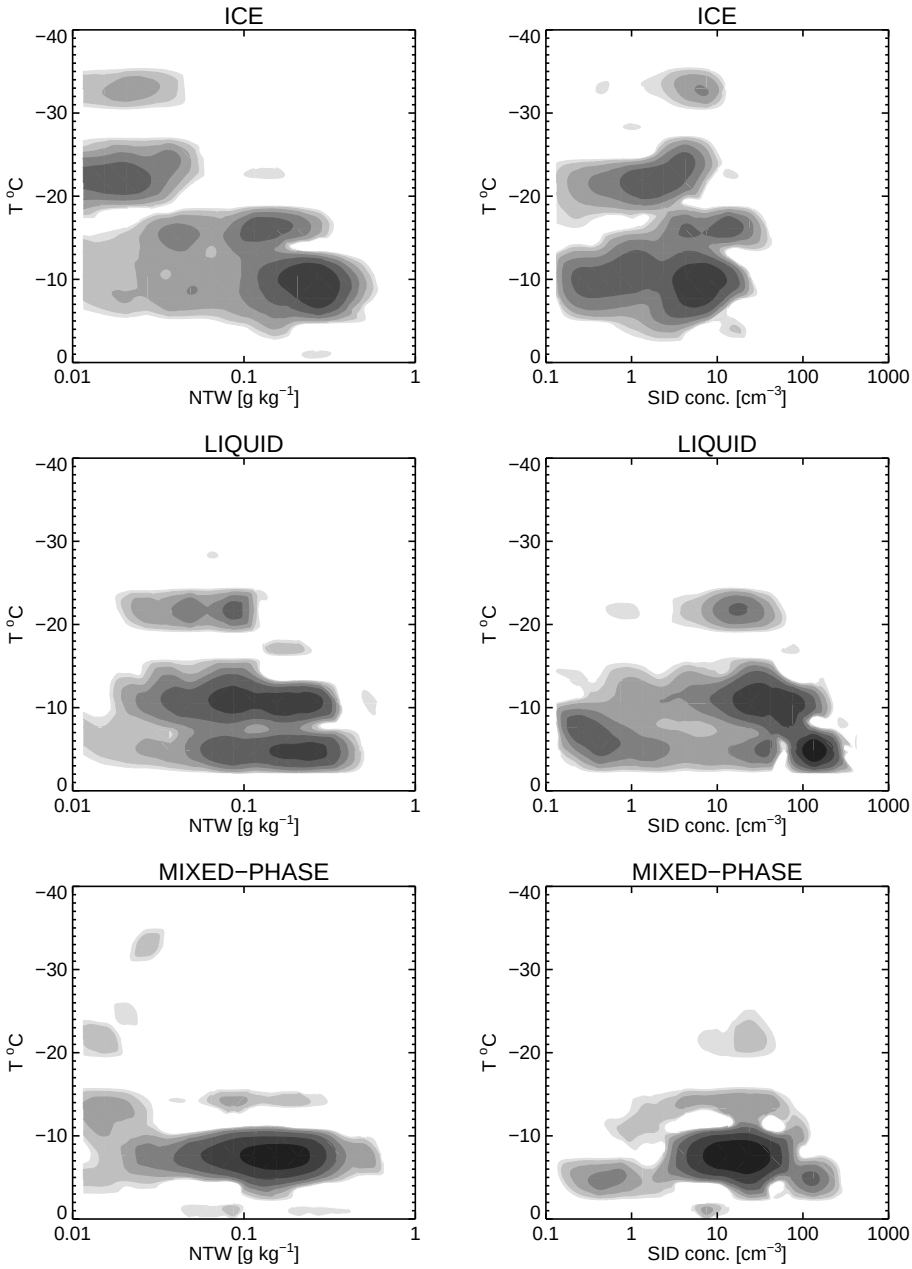

Figure 20. Plots of condensed water contents from the Nevzorov probe and concentrations from the SID probe encountered over the three flights. The contours (see fig 4 for contour values) represent the bin normalised concentration: (number in bin)/(N), where for [topleft] N=5570, dx=0.13,dy=2.8; [topright] N=8416, dx=0.25, dy=2.8; [midleft] N=1442, dx=0.13, dy=2.8; [midright] N=2517, dx=0.25, dy=2.8; [bottomleft] N=1214, dx=0.13, dy=2.8; [bottomright] N=1404, dx=0.25,dy=2.8. These plots are derived from 1-s data.

ties of the SID and FSSP probes and may help explain the differences observed between concentrations in the ice regions.

8. Conclusions

Three flights in mixed-phase conditions were carried out in conjunction with the Chilbolton radar as part of the NERC CWVC thematic program. The following results were found:

- Particle sphericity appears to be a good indication of phase in these types of cloud where any newly produced ice will quickly grow in highly ice supersaturated conditions into non-spherical particles, although on one occasion it appeared that spherical ice particles were being sampled and so the shape measured by SID may not always be a faultless indicator of phase.

- The Nevzorov NLW/NTW ratio and SID spherical fraction generally show a positive correlation. However, SID can indicate a high spherical fraction even when the Nevzorov probe shows a low NLW/NTW ratio. This is due to the fact that SID is inherently concentration based whereas the Nevzorov probe looks at the mass-weighted fraction.

- The residual signal for the Nevzorov liquid water sensor when operating in ice conditions on the UK C-130 is 18% of the 1-s averaged Nevzorov Total Water sensor for true air speeds in the range 100-120 m s^{-1}.

- Using just three flights (~1200 km) produces a concentration weighted liquid fraction from the SID that is in agreement with previous work. We find that liquid occurs 40% of the time in clouds between -5 and -10C, falling to 20% for temperatures between -10 and -15C. We find a maximum in the frequency of mixed-phase intervals encountered of 19% between -5 and -10C.

- Regions of supercooled liquid water and/or mixed-phase on scales as short as 100m were observed.

- High ZDR values can be indicative of the nearby presence of liquid water giving rise to highly ice saturated conditions conducive to the growth of columnar or planar crystals with high axial ratios. Although this is the case for discrete cloud layers it is not always true within a deep frontal cloud where aggregates falling from above can supress the high ZDR signal. Therefore, while the presence of high ZDR (greater than around 2 dB) above the melting layer is almost always indicative of the presence of supercooled water, the absence of high ZDR does not necessarily point to an absence of supercooled liquid water. Hence, when aggregation (diffusional growth) dominates the ice crystal morphology the ZDR signal is weak (strong).

Future work will involve the extension of sampling to a wider dataset and target clouds that are not necessarily expected to contain large amounts of supercooled liquid water. A larger dataset will allow a better analysis of the scale dependence of supercooled liquid, ice and mixed-phase clouds. Further investigation is required of the preferential

location of narrow layers of supercooled water near cloud top because they are difficult to resolve in numerical climate models but will have a strong radiative impact. New insight into the phase structure of cumulus clouds could be provided by the ability demonstrated here to probe the high resolution structure mixed-phase clouds.

ACKNOWLEDGEMENTS

The authors wishes to thank the staff of MRF and the RAF C-130 aircrew for their assistance and hard work and we are grateful to the Radio Communications Research Unit at the Rutherford Appleton Laboratory for the use of the Chilbolton radar facility. The CWVC experiment was funded by The UK Natural Environment Research Council, under grants GST/02/2874 and T/S/2000/01023.

REFERENCES

Cober S. G., Isaac G. A., Korolev A. V., Strapp J. W., 2001:Assessing cloud-phase conditions J. App. Met., 40 (11), 1967-1983.

Bower KN, Moss SJ, Johnson DW, Choularton TW, Latham J, Brown PRA, Blyth AM, Cardwell J, 1996: A parametrization of the ice water content observed in frontal and convective clouds Quarterly Journal of the Royal Meteorological Society, 122 (536), 1815-1844.

Dye, J. E. and Baumgardner, D., 1984: Evaluation of the Forward Scattering Spectrometer Probe. Part I: Electronic and Optical Studies. J. Atmos. Oceanic Technol., 1, 329-344.

Field, P. R., Wood, R., Brown, P. R. A., Kaye, P. H., Hirst, E., Greenaway, R., Smith, J. A., 2003: Ice particle interarrival times measured with a fast FSSP. J. Atmos. Ocean. Technol., 20(2), 249-261.

Fleishauer R. P., Larson V. E., Vonder Haar T. H., 2002: Observed microphysical structure of midlevel, mixed-phase clouds J. Atmos. Sci., 59(11), 1779-1804.

Goddard, J. W. F., Eastment J. D. and Thurai, M.1994: The Chilbolton advanced meteorological radar - a tool for multidisciplinary atmospheric research. Electron. Commun. Eng. 6 (2) 77-86.

Hirst E., Kaye P. H., Greenaway R. S., Field P. R., and Johnson D. W., 2001: Discrimination of micrometre-sized ice and super-cooled droplets in mixed-phase cloud. Atmos. Environ. 35 33-47.

Hogan, R. J., P. N. Francis, H. Flentje, A. J. Illingworth, M. Quante and J. Pelon., 2003a: Characteristics of mixed-phase clouds: Part I: Lidar, radar and aircraft observations from CLARE'98 Quart. J. Roy. Meteorol. Soc., in press.

Hogan, R. J., A. J. Illingworth, E. J. O'Connor and J. P. V. Poiares Baptista. 2003b: Characteristics of mixed-phase clouds: Part II: A climatology from ground-based lidar Quart. J. Roy. Meteorol. Soc., in press.

Hogan, R. J., P. R. Field, A. J. Illingworth, R. J. Cotton and T. W. Choularton, 2002: Properties of embedded convection in warm-frontal mixed-phase cloud from aircraft and polarimetric radar Quart. J. Roy. Meteorol. Soc., 128, 451-476.

Jourdan O., Oshchepkov S., Gayet J-F, 2003: Statistical analysis of cloud light scattering and microphysical properties obtained from airborne measurements. J. Geophys. Res. 108(D5), 4155, AAC1-6.

Knollenberg, R. G., The optical array; an alternative to scattering or extinction for airborne particle size determination. J. Appl. Meteor. 1970, 9, 86-103

Korolev, A. V. and Strapp, J. W. and Isaac, G. W. and Nevzorov, A. N. The Nevzorov airborne hot-wire LWC-TWC probe: Principle of operation and performance statistics. J. Atmos. Ocean. Tech. 1998, 15, 1495-1510.

Korolev A. V., Isaac G. A., Cober S. G., Strapp J. W. and Hallett J., 2003: Microphysical characterization of mixed-phase clouds. Q. J. R. Meteorol. Soc., 129, 39-65.

Korolev A. V. and Mazin, I. P., 2003: Superaturation of water vapor in clouds. J. Atmos. Sci., in press.

Lawson R. P., Baker B. A., Schmitt C. G., Jensen T. L., 2001: An overview of microphysical properties of Arctic clouds observed in May and July 1998 during FIRE ACE J. Geophys. Res., 106 (D14), 14989-15014.

Moss S. J. and Johnson D. W., 1994: Aircraft measurements to validate and improve numerical model parametrisations of ice and water ratios in clouds. Atmos. Res. 34, 1-25.

Nichols S., Leighton J. and Barker R., 1990: A new fast response instrument for measuring total water content from aircraft. J. Atmos. Oceanic Technol., 7, 706-718.

Pinto J. O., Curry J. A., Intrieri J. M., 2001: Cloud-aerosol interactions during autumn over Beaufort Sea J. Geophys. Res., 106 (D14), 15077-15097

Strapp J. W., Oldenburg J., Ide R., Lilie L., Bacic S., Vukovic Z., Oleskiw M., Miller D., Emery E. and Leone G., 2003 Wind Tunnel Measurements of the Response of Hot-Wire Liquid Water Content Instruments to Large Droplets. J. Atmos. Sci. 20, 791-806.

Wood R. and P. R. Field, 2000: Relationships between total water, condensed water and cloud fraction exam ined using aircraft data. J. Atmos. Sci., 57, 1888-1905.